A Unified View-Graph Selection Framework for Structure from Motion

Rajvi Shah Visesh Chari P J Narayanan
Center for Visual Information Technology, IIIT Hyderabad, India
{rajvi.shah@research.iiit.ac.in, visesh@gmail.com, pjn@iiit.ac.in}

Abstract

View-graph is an essential input to large-scale structure from motion (SfM) pipelines. Accuracy and efficiency of large-scale SfM is crucially dependent on the input view-graph. Inconsistent or inaccurate edges can lead to inferior or wrong reconstruction. Most SfM methods remove 'undesirable' images and pairs using several, fixed heuristic criteria, while the subgraph selection often depends on the dataset. We present a new optimization framework for view-graph selection to achieve different reconstruction objectives and propose a very efficient network-flow based formulation for its approximate solution. Different selection objectives can be achieved by varying the influence of the cost terms that are derived from local priors such as connectivity, overlap, baseline, ambiguity, loop consistency, etc. We show encouraging results on popular landmarks datasets and on highly ambiguous datasets involving symmetry and large duplicate structures using novel priors.

1. Introduction

Large-scale structure from motion (SfM) based 3D reconstruction has matured significantly to achieve even city-scale reconstructions automatically [1, 4, 14]. These reconstruction pipelines have to find visual correspondences between images automatically and remove noisy or unwanted images/pairs prior to or during reconstruction. A match-graph (MG) with images as nodes and pairs that share putative matches as edges is constructed first. A view-graph (VG) is a subset of the match-graph where edges represent valid epipolar geometries (EGs) between nodes they connect. View-graphs help in 'organizing' unordered image collections useful to (i) select a core set of images for reconstruction and (ii) identify noisy EGs that might degrade the quality of reconstruction. State-of-the-art SfM methods like incremental [24, 34, 21], hierarchical [5, 9, 30], or global [23, 3, 18, 17, 2], all consist of a view-graph based initial step for ordering and pruning images.

SfM methods use a subgraph of the initial VG for actual reconstruction for mainly efficiency and accuracy. Using the full VG for SfM is often computationally expensive and unnecessary due to the high redundancy in the image set. Due to cubic complexity of incremental bundle adjustment (BA), large-scale incremental SfM pipelines solve the core reconstruction problem on smaller subgraphs, such as skeletal graphs [1, 26] or iconic scene graphs [4, 19]. Though the BA bottleneck has improved with near linear time incremental methods [34, 21], it still remains very important to select 'good' images and more importantly 'good' pairs for accurate reconstruction.

Large community photo collections often display point-of-view bias, as some viewing angles are more popular than others. Images with high visual overlap are strong pairs in the MG with large number of inliers. However, for closely clustered images, such narrow baseline pairs increase the uncertainty of triangulation, causing large re-projection errors. While isolated erroneous EGs can be overcome by robust averaging (global SfM) and repeated bundle adjustment (incremental SfM), large number or incorrect or ill-conditioned EGs can result in incorrect reconstruction. Ambiguous scenes with symmetric or duplicate structures often fail with mis-registered cameras, or folded structures (in the form of 'phantom' structures, or structures incorrectly folded along symmetry). Methods proposed to handle such difficult scenes use global reasoning with priors based on missing correspondences [36, 20, 15] or conflicting observations [12, 13]. Summarily, the problem of VG filtering is important for various reasons and is tackled in many different ways across SfM methods.

The main motivation of our work is to formalize view-graph selection as an optimization problem to bring greater flexibility and control to it. To filter input view-graphs, SfM methods typically leverage conservative heuristics on inliers, baselines, homography, loop consistency, etc. While these heuristics work well for a large variety of datasets, it is not straightforward to adapt these heuristics to specific datasets and problems. With this as motivation, we introduce a method to meet many different subgraph selection objectives using a unified framework. We formalize view-graph selection as an optimization problem and propose a novel network-flow based formulation for its efficient approximate solution. Costs in the proposed optimization ob-

jective are modeled as a combination of several local geometry based priors. Varying the priors and their combinations can allow to encode a variety of objectives. The focus of this paper is not an exhaustive study of all possibilities, but presenting a flexible framework that allows different objectives to be modeled by plugging in/out appropriate priors for an 'optimal' selection. In this paper, we focus on two objectives, (i) accuracy, and (ii) disambiguation, discuss existing and new priors for these objectives, and achieve accurate and ghost-free reconstructions on a variety of challenging datasets. To the best of our knowledge, this is the first attempt at systematizing view-graph selection.

2. Related Work

View-graph selection is an implicit part of many SfM methods in form of thresholds on various criteria for filtering out undesirable images and pairs. Many methods are also proposed to find the optimal subgraph for specific reconstruction objectives. We first briefly revisit the implicit criteria employed by traditional SfM methods and later discuss the optimal subgraph selection methods.

2.1. View-graph Filtering

View-graph filtering in Incremental SfM Accuracy and completeness of incremental SfM hinges on seed pairwise reconstruction and next best view selection. Wide baseline seed pair selection is ensured using criteria based on epipolar inliers that don't fit a homography [24, 25], or categorization of pairwise motion as planar, rotational, or general using various inlier ratios [21]. For next best view selection, triangulation angle, number of inliers, or correspondence distribution statistics are used as criteria [24, 21].

View-graph filtering in Global SfM Global SfM methods estimate global rotations using relative rotation estimates and then estimate global translations [23, 3, 17, 2, 32, 29]. In [3], to reduce the state space of camera parameters for MRF based estimation, relative twist ($> 20°$) and unusual aspect ratios are used as the view filtering criteria. Methods that use lie-algebraic averaging of relative rotations [6, 7, 35, 18, 17, 2, 29] for global rotation estimation often discard images with unknown calibration and handle outlier EGs with loop consistency constraints [35, 18, 17] and robust cost formulations.

View-graph filtering for ambiguous scenes Scenes with large duplicate structures or symmetries are particularly difficult to reconstruct since the full view-graph has many outliers. Due to self-similarity many EGs are incorrect yet form consistent loops, making simple consistency checks insufficient for view-graph filtering. Missing correspondeces based heuristics are useful to identify erroneous pairs in such scenes [36, 20]. In gist, missing correspondeces mean that if in a view-triplet features matched between two images do not match the third, it is likely that the third image captures a different instance than the first two. In [15], this prior is computed in a global context and the view-graph is grown in a consistent manner, starting from a spanning tree. Another approach [12, 13] is to correct the wrong reconstruction of an ambiguous scene in a post-processing step. This approach relies on a prior based on co-visibilities of 3D points and conflicting observations.

Many of the heuristics and criteria discussed above can be easily incorporated as unary and pairwise costs for image and pairwise selection into our framework. Other heuristics that employ global inference (such as loop consistency) can be approximately incorporated as a pairwise heuristic. For disambiguation, we propose a context based pairwise selection prior that is based on both, missing correspondences and conflicting observations. Unlike [12], this prior can be computed before reconstruction and the proposed optimization is very efficient.

2.2. Finding the Optimal Subgraph

Many methods have been proposed for finding an optimal subgraph from the full VG to meet various objectives. For efficiency and completeness, incremental/hierarchical SfM methods use optimal subgraphs such as skeletal graph [26], iconic scene graph [19], min. connected dominating sets [11], dendograms [30], etc. The methods for finding these subgraphs differ in their objectives as well as selection strategies. For global methods, incremental BA is not the efficiency bottleneck, hence optimal subgraphs are often related to consistency and robustness goals. Global methods use specialized solutions such as inference on graph with consistency based priors [17, 35], random sampling of spanning trees [7, 18] with consistent edge addition, and local convexity based sub-division [33]. In [29], EGs in a view-graph are directly refined by minimizing a triplet reprojection error based objective using a large non-linear optimization. For efficiency, they choose a spanning subgraph such that each edge participates in at least one triplet. Our framework should not be seen as a one-size-fits-all replacement of these specialized methods tailored to one particular objective. Our focus is on exploring an efficient and generalized, optimization based selection framework which makes it possible to plug in and plug out various selection priors to meet different objectives.

Recently, a fast graph-based matching approach is proposed to build consistent view-graphs that achieve accurate reconstruction on both general and ambiguous scenes. While, we also demonstrate utility of our approach with disambiguation as an objective, the focus of our work is not feature matching but unified view-graph selection. Hence, our approach to the problem is entirely different.

3. Notation and Problem Formulation

Let the input view-graph be $\mathcal{G} = (\mathcal{V}, \mathcal{E})$, where the set of vertices (nodes) $\mathcal{V}$ represents the images and the set of edges $\mathcal{E}$ represents the pairwise epipolar geometries (EGs). The goal is to select a subset of nodes $\mathcal{V}'$ and a subset of edges $\mathcal{E}'$ (a subgraph $\mathcal{G}' = (\mathcal{V}', \mathcal{E}')$) that meets a desired objective. We denote the indicator variables for image selection as δ_i and pair selection as δ_{ij}. Here, each δ_i corresponds to the image vertex $v_i \in \mathcal{V}$ and each δ_{ij} corresponds to the pairwise edge $e_{ij} \in \mathcal{E}$. The selection problem can be represented as a minimization of the following form,

$$\begin{array}{ll} \arg\min & f(\delta) = c_i\delta_i + c_{ij}\delta_{ij} \\ \text{subject to} & \sum \delta_i \leq N, \sum \delta_{ij} \leq M \\ & i \in \mathcal{V},\ (i,j) \in \mathcal{E},\ \delta_i, \delta_{ij} \in \{0,1\}. \end{array} \tag{1}$$

Activation of indicator variables δ_i and δ_{ij} imply selection of the corresponding image v_i and pair e_{ij}. c_i is the cost of selecting the view v_i and c_{ij} is the cost of selecting e_{ij}. Modeling these costs using different priors and their combinations can allow us to achieve different selection objectives. In the next section, we discuss cost modeling for accurate and ghost-free reconstructions using a few select priors. However, a variety of other priors known in SfM literature can also be incorporated in this formulation to achieve different objectives.

This representation is slightly problematic, since selection of images and pairs is not independent. Since, each image is most likely connected to more than one image, activation of selection variables δ_i and δ_j does not necessarily imply selection of the image pair (i, j). On the contrary, selection of image pair (i, j) implies that both images i and j constituting the pair must be selected. We model this dependency by adding additional constraints to the minimization.

$$\begin{array}{ll} \arg\min & f(\delta) = c_i\delta_i + c_{ij}\delta_{ij} \\ \text{subject to} & \sum \delta_i \leq N, \sum \delta_{ij} \leq M \\ & \forall i,j\ \delta_{ij} \leq \delta_i,\ \delta_{ij} \leq \delta_j,\ \delta_i + \delta_j - \delta_{ij} \leq 1 \\ & i \in \mathcal{V},\ (i,j) \in \mathcal{E},\ \delta_i, \delta_{ij} \in \{0,1\}. \end{array} \tag{2}$$

The optimal solution of this minimization problem can be obtained by binary integer linear programming, but it is NP-complete. A standard trick is to use linear programming (LP) relaxation and obtain a binary solution by rounding the values to {0,1}. However, in our experiments, this approach often lead to random assignments due to values close to 0.5. Instead, we approximate this optimization problem as a minimum cost network-flow problem that guarantees us a binary solution in polynomial time. In the next sections, we first explain how we model the image selection and pairwise selection costs c_i and c_{ij} and later explain our formulation of view-graph selection as minimum cost network flow (MCNF) problem (more on this is discussed in *supplementary material*).

4. Cost Modeling

Costs in the proposed optimization indicate an image or an EG's fitness for a given objective. For our experiments, we model costs based on a few graph-based and local geometry based priors. However, many additional image-based or extrinsic priors can also be incorporated in our framework for other objectives.

4.1. Image Selection Priors

Fitness of an image in the view-graph can be described by many factors. For the purposes of accurate and complete reconstruction, we consider three priors, (i) degree of an image in the view-graph, (ii) fraction of an image's features that participates in tracks, (iii) local clustering coefficient of an image. Degree of the vertex (images) in the view-graph and feature connectivity are useful measures to select images with many observations and connections. Images with high degree are well-connected and their features will likely form longer tracks useful for accurate triangulation. Since internet photo collections often suffer from point of view bias, only degree based image selection will likely lead to only popular components. Hence, we include local clustering coefficient (lcc) of a vertex as an image prior to prefer images that provide connections across components than within components. The image selection cost is a combination of such individual priors of the form, $c_i = \sum_k \alpha_k f_k(i)$.

Additionally, other priors such as availability of calibration information, unusual aspect ratio, relative twist, distribution of features in the image etc. can also be used for cost modeling for different selection objectives.

4.2. Pairwise Selection Priors

Fitness of the pairwise geometries (EGs) hold more importance for accuracy and disambiguation objectives. We use six (existing and new) priors to model pairwise selection costs as a linear combination of the form $c_{ij} = \sum_k \beta_k f_k(e_{ij})$ in our experiments. Many additional pairwise priors, such as ordering information based on GPS or timestamps can also be incorporated in the proposed formulation. We use the following notations to later explain the pairwise selection priors.

Notation: For image pair $(\mathrm{I_i}, \mathrm{I_j})$, the sets of all matched features (matched with any other image) are S_i, S_j and the sets of features that match between $(\mathrm{I_i}, \mathrm{I_j})$ are M_i, M_j. The difference sets $U_i = S_i \setminus M_i$, and $U_j = S_j \setminus M_j$ consist of unique features in $\mathrm{I_i}$ and $\mathrm{I_j}$. With slight abuse of notation, the area of a convex hull of a set P is denoted as $\mathbb{A}(P)$.

Overlap is defined in terms of fraction of image $\mathrm{I_i}$'s total matchable area covered by features that match with image $\mathrm{I_j}$. We compute this as sum of ratios of convex hull areas, $f_1(i,j) = g_1(\frac{\mathbb{A}(M_i)}{\mathbb{A}(S_i)} + \frac{\mathbb{A}(M_j)}{\mathbb{A}(S_j)})$.

(a) $\Delta R_\theta = 2°, \Delta C_\theta = 4°$ (b) $\Delta R_\theta = 2°, \Delta C_\theta = 119°$

Figure 1: Examples pairs where multiple motions are detected. While for pair (a) the primary and secondary rotations and positions are in agreement, for pair (b) the ambiguity is clearly reflected in position difference.

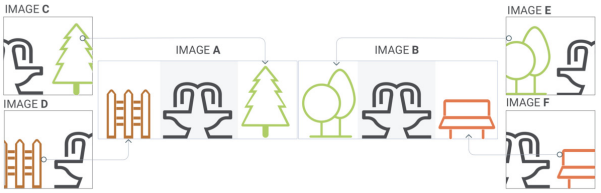

Figure 2: Image pair (A,B) capture a scene with duplicate elements. Though duplicate elements in the images yield many matches, elements in context regions tend to find matches with non-intersecting sets of images.

Median triangulation angle between triangulated correspondences is a useful prior about baseline of the EG, $f_2(e_{ij}) = g_2(\tilde{\theta}_{ij})$, $\theta_{ij} = \{\angle(\text{ray}(m_i), \text{ray}(m_j))\}$

Infinite homography Image pairs with panoramic motion (rotation around a fixed center) tend to have high overlap but are undesirable for reconstruction as they lead to degenerate or ill-conditioned EG. Simply using homography inliers will also reject valid pairs that capture planar regions. We use the fact that calibration normalized infinite homographies are basically rotations [8]. Hence, $\mathrm{H}^\mathsf{T}\mathrm{H}$ should be close to identity for such pairs. We base our homography prior on this assumption as, $f_3(e_{ij}) = g_3(||\mathrm{H}_{ij}^\mathsf{T}\mathrm{H}_{ij} - \mathrm{I}||_\mathrm{F})$. We don't use this prior for uncalibrated images.

Multiple motions We model this prior to disambiguate image pairs capturing repetitive or duplicate instances of some scene elements. We remove the correspondences that satisfy the estimated EG from the initial set of matches and estimate the secondary relative pose using the leftover matches. If sufficient inliers are found, we decompose the relative pose into rotation and translation. We estimate the angular difference between primary and secondary rotations and also the angle between the both position vectors. If the difference angles are small, the secondary motion is most possibly arising due to threshold sensitivity and measurement drift, otherwise, these indicate presence of correspondences on ambiguous structures. Examples for both these scenarios are shown in Figure 1. For motions other than along the direction of repetition, this measure is effective. $f_4(e_{ij}) = g_4(\Delta R_\theta, \arccos(\Delta \mathrm{c}_{ij}^\mathsf{T} \Delta \mathrm{c}_{ij}))$.

Loop consistency Loop consistency suggests that rotations in an EG triplet when chained should yield identity [8]. We find all triplets in the view-graph and label them as consistent or inconsistent. For each EG, we count the total number of consistent EGs it participates in and use this as a measure of its fitness. Though it is not same as explicitly enforcing loop consistency, it is a convenient way to incorporate a non-local (pairwise) geometric cue as a pairwise prior. $f_5(e_{ij}) = g_5(\frac{\text{\# consistent triplets on } (i,j)}{median(\text{\# consistent triplets on any}(i,j))})$.

Context Similarity Missing correspondences (matches in a pair, not matching the third image in a triplet) are a useful prior for disambiguation in presence of duplicate structures [36, 20, 15]. However, by itself it is not sufficient for disambiguation and it is commonly used in an inference framework or with a global objective. Track covisibility statistics computed using social networking principles are also found useful for disambiguation [31], but it is not straightforward to apply this prior to describe pairwise fitness. In a post-reconstruction disambiguation approach [13], reconstructed 3D points are back-projected into image pairs and conflicting observations in unmatched regions (context) are identified. However, this measure is also not directly useful as our approach is aimed to work before reconstruction. Motivated by these, we propose a new, context based, pairwise prior suitable for our framework.

Suppose images I_i and I_j are looking at a scene with duplicate instances of a structure. The features in the match sets M_i and M_j will most likely lie on the duplicate elements. We consider the unique feature sets U_i and U_j to belong to the context regions. Recall that U_i and U_j consist of features that match other images in the collection and not I_j, I_i. If two images are truly looking at the same instance, the context features of both images would have matched similar set of images. On the other hand, if two images are looking at duplicate instances, the context features would be distributed over different sets of images. We find distribution of features in U_i and U_j over all N images in the collection based on their matches and make an N dimensional description of the context space. This concept is illustrated in Figure 2. Context feature of image I_i w.r.t. image I_j can be described as $\mathbf{w}_{ij} = [w_i^1, w_i^2, \ldots, w_i^N] \quad w_i^j = 0$, where $w_i^k = |\{u \in U_i \mid u \leftrightarrow u', u' \in S_k, k \neq j\}|$. This measure is biased against pairs with very low visual overlap, however, along with other measures, it works effectively for selection. We compare the context features of a pair using cosine similarity or hamming distance (after binarization). For small datasets, cosine similarity works better, but for large datasets, both measures perform similarly. The context similarity can be defined as, $f_6(e_{ij}) = g_6(\mathbf{w}_{ij}^\mathsf{T}\mathbf{w}_{ij})$.

Prior normalization and weighting In cost equations for each prior, g_k represents the normalization applied on the raw prior value. Depending on the end objective, different priors need to be normalized differently, i.e. high value of overlap, medium value of triangulation, high value of lcc are undesirable for accurate reconstruction. The weighing coefficients (α_k, β_k) decide the importance of individual prior in overall cost. In our experiments, we use uniform values for (α_k, β_k) which work well across all datasets. Learning the normalization and optimal weights for combination is an interesting but non-trivial future problem.

5. View-graph Selection as MCNF Problem

We now explain the proposed formulation that allows us to approximate the optimization introduced in section 3 as a minimum cost network flow (MCNF) problem. The network in MCNF problems is a directed graph with at least one source and one sink nodes. We denote the network as $\mathcal{T} = (\mathcal{N}, \mathcal{A})$, where $\mathcal{N}$ represents the set of nodes and $\mathcal{A}$ represents the set of directed edges/arcs. Each edge (i, j) in the network has a cost c_{ij} associated to let across one unit of flow, and the cost incurred by an edge is proportional to the flow (x_{ij}) through it. Each edge also has a lower and an upper bound (l_{ij}, u_{ij}) on the amount of flow (x_{ij}) that can pass through it, known as **capacity constraints**. The source sends a certain units of flow that the sink node must receive. At all other nodes, flow must be conserved, i.e. the total incoming and outgoing flows must be equal. Let us denote the total flow as F and the remainder flow at a node i as b_i, then $b_i = F$ when i is source, $b_i = -F$ when i is sink, and $b_i = 0$ otherwise. These constraints are known as **equal flow constraints**. The MCNF problem is about sending the total flow from the source node to the sink node at a minimum cost, without violating the capacity and flow constraints. This minimization with flow and capacity constraints can be described as follows,

$$\begin{aligned} &\text{Minimize} && \text{Subject to,} \\ &\sum_{(i,j)\in\mathcal{A}} c_{ij}x_{ij} && l_{ij} \le x_{ij} \le u_{ij} && \forall (i,j) \in \mathcal{A} \\ & && \sum_{\{j:(i,j)\in\mathcal{A}\}} x_{ij} - \sum_{\{j:(j,i)\in\mathcal{A}\}} x_{ji} = b_i && \forall i \in \mathcal{N} \end{aligned} \tag{3}$$

Network construction To pose view-graph selection as an MCNF problem, we first construct the network as follows. All indicator variables corresponding to selection of views $\{\delta_i\}$, and pairwise geometries $\{\delta_{ij}\}$ are represented using arcs/edges $(i, j) \in \mathcal{A}$ in the network, source and sink nodes are auxiliary. Since view selection variables are represented as arcs, each vertex i in the view-graph corresponds to two nodes, $(2i-1, 2i)$ in the network. Each odd node $(2i-1)$ corresponding to the vertex i in the view-graph is connected to the source node and similarly each even node $(2i)$ is connected to the sink node. The arcs corresponding to the pairwise selection variables $\{\delta_{ij}\}$, join the even node of the lower index image with the odd node of the higher index image. This choice prevents cycle formation in the network. Summarizing, the network consists of $|\mathcal{N}| = 2|\mathcal{V}| + 2$ nodes and $|\mathcal{A}| = |3\mathcal{V}| + |\mathcal{E}|$ arcs. These arc connections in the network are summarized in Figure 3 along with a pictorial example.

Edge Type	Connected Nodes		Capacity
Source:	$(0, 2i-1)$	$\forall i \in \mathcal{V}, 0$: source	$[0, F]$
Sink:	$(2i, \lvert\mathcal{V}\rvert+1)$	$\forall i \in \mathcal{V}, \lvert\mathcal{V}\rvert+1$: sink	$[0, F]$
Image:	$(2i-1, 2i)$	$\forall i \in \mathcal{V}$	$[0, \text{degree}(i)]$
Pairwise:	$(2i, 2j-1)$,	$\forall e(i,j) \in \mathcal{E}, i < j$	$[0, 1]$

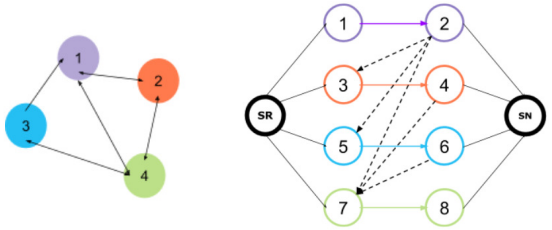

(a) View-graph (b) Network formulation

Figure 3: The table describes the edge/arc connections in the network based on VG vertices and edges. The figure on the bottom shows an example network construction (right), for a sample view-graph shown on the left. Source and sink nodes are depicted by black outline. Image nodes in the VG and the corresponding selection edges in the VG are depicted by color-coded outlines (see in color). Pairwise edges are depicted by black dashed lines.

Equal flow and capacity constraints At source and sink the sent and received flow is equal to the total flow. Equal flow constraints require that in and out flow at every other node remain equal. In our formulation, capacity constraints - lower and upper bounds on flow through an arc are specified based on the edge type as mentioned in Figure 3.

To understand the choice of these capacities, consider the vertex v_1 in the depicted view-graph. The arc corresponding to v_1's selection variable δ_1 in the network is $a(1, 2)$. Corresponding to v_1's degree in the VG, the node n_2 in the network has three outgoing arcs $a(2, 3)$, $a(2, 5)$, and $a(2, 7)$ for pairwise selection variables δ_{12}, δ_{13}, and δ_{14}. The flow starting from source node, after passing through $a(1, 2)$, should plausibly be able to pass through all three outgoing arcs. Since flow can only be divided in integer units, the minimum capacity of image selection arc $a(1, 2)$ has to be at least 3 ($deg(v_i)$). Under minimum cost solution, the flow at any node will continue to take the path of least resistance (cost). Now, suppose that the cost assigned to $a(2, 3)$ is the least amongst the three outgoing arcs and its max. capacity is 3 units (or any value $1 < k < deg(v_i)$). In this sce-

nario, $a(2,3)$ being the lowest cost arcs will pull all 3 units of flow from $a(1,2)$, starving the other arcs of any flow and preventing the corresponding view-graph edges from ever getting selected. To avoid this, we restrict the maximum flow through pairwise selection arcs to 1.

Effect of cost range on solution In minimization sense, negative costs provide encouragement for flow to pass through an arc, whereas positive costs provide discouragement. Suppose, all costs are negative, then total flow F of 1 unit will select the lowest cost chain in the network (often the longest). As we increase the value of total flow, more paths get explored and when $F = |\mathcal{E}|$ all images and EGs get selected. When costs are both encouraging and discouraging, many positive cost arcs will act as barriers for the flow. As a result, at some value of total flow F the selection will (nearly) saturate and may never select the full view-graph. All results shown in this paper are obtained using only negative (encouraging) costs, $(-1 \leq c_{ij} \leq 0)$.

Effect of total flow on solution Total flow is a free parameter in the proposed MCNF solution. To systematically understand the effect of total flow on image and pair selection, we created synthetic view-graphs with varying number of vertices, varying degrees of connectivity, and randomly assigned (negative) costs. The connectivity across vertices is simulated using Gaussian assumptions on neighborhood (detail in the suppl. material). We performed sub-graph selection on $\sim$100 synthetic view-graphs using proposed MCNF approach for increasing value of total flow and observed consistent selection behavior. Figure 4 shows the fraction of total EGs selected vs. normalized total flow on regular scale (left) and logarithmic scale (right). It can be seen that for negative costs, the relation between total flow and selected EGs is logarithmic. This relation is also observed on view-graphs of real-world scenes (see in suppl. material). We fit a polynomial curve to this distribution to parameterize total flow selection. Practically, we specified the number of EGs desired in the selected sub-graph and sampled the corresponding value of total flow using the fitted curve and obtained satisfactory results.

Running time A main advantage of this formulation is that it can be solved very efficiently. Constructing the network and solving for MCNF takes less than 2-3 seconds even for graphs with $\sim$1000 nodes and $\sim$100K edges.

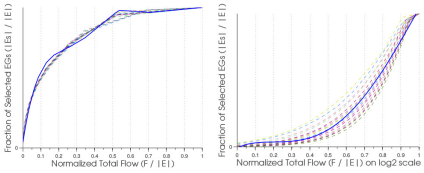

Figure 4: Effect of total flow on pairwise selection

6. Results and Discussion

The proposed selection framework is versatile and can be used in multiple ways to model different objectives using costs modeled using relevant priors. Since, this is an introductory work, we apply our framework for two objectives, *accuracy* and *disambiguation* and show results on these datasets, *(i)* MVS benchmark [27], *(ii)* small ambiguous scenes [20], *(iii)* large ambiguous scenes (from [13, 22]), and *(iv)* Internet landmarks (from [24, 16]). Datasets *(i,ii)* consist of small scenes with $\sim$10 - 60 images. Number of images in datasets *(iii,iv)* are listed in Table 3a. For all results shown in this paper, we used uniform weights to combine all priors mentioned in section 4. Implementation details are provided in supplementary material.

			Incremental SfM			Global SfM		
Dataset	VG	$\|\mathcal{E}\|$	R_{err}	T_{err}	r_{err}	R_{err}	T_{err}	r_{err}
Castle30	S	49	2.44	0.15	0.38	2.21	1.29	1.01
	F	118	2.22	0.22	0.34	2.17	7.49	1.14
Fountain11	S	21	2.90	0.01	0.29	2.82	0.29	0.35
	F	25	2.90	0.01	0.72	2.82	0.27	0.59
Herzjesu25	S	55	2.36	0.03	0.50	2.38	0.75	1.18
	F	128	2.38	0.02	0.43	2.39	0.56	1.71

Table 1: View-graph selection and reconstruction statistics for MVS benchmark datasets. Labels 'S' and 'F' indicate selected and full subgraphs. R_{err}, T_{err}, and r_{err} indicate median rotation, translation, and reprojection errors. Total flow value was chosen to select 50% of total EGs. Reconstructions with selected VGs achieve better or comparable accuracy to those with full VGs.

Dataset	VG	$\|\mathcal{V}_s\|$	$\|\mathcal{E}_s\|$	t_{sel}	N_c	r_{err}	R_{err}	T_{err}	t_{sfm}
Notre Dame	S	752	11307	0.517	741	1.016	0.089	0.319	1274.53
	F	781	139630	0.825	775	1.313	0.112	0.308	3601.65
Pantheon	S	646	12331	0.331	617	1.327	0.090	0.216	1124.83
	F	714	46746	0.323	682	1.503	0.089	0.217	1760.81
St. Peters	S	1105	20846	0.642	1067	1.211	0.037	0.577	1121.92
	F	1155	119977	0.713	1111	1.458	0.028	0.496	1367.71

Table 2: View-graph selection and reconstruction statistics for three popular landmark datasets. Reconstruction for selected view-graph (indicated by 'S') is performed using global SfM pipeline [28]. In absence of ground-truth, we compare reconstruction accuracy by comparing with incremental SfM based baseline reconstructions with full view-graphs (indicated by 'F'). Both reconstructions are RANSAC aligned. $|\mathcal{V}_s|$, $|\mathcal{E}_s|$ indicate selected vertices and edges, t_{sel} indicate time taken by MCNF, N_c shows number of reconstructed cameras, r_{err} , R_{err} , T_{err} indicate reprojection, rotation, translation errors, t_{sfm} is the time taken by SfM. Total flow values were chosen corresponding to $|\mathcal{E}_s| = |\mathcal{V}| \times 10$. The reconstructions of selected VGs maintain good accuracy and expectedly take shorter time. Qualitative results are shown in the supplementary material.

Figure 5 shows the reconstruction results for small ambiguous scenes dataset[20]. This set has 2 more scenes ('indoor' & 'building') that get reconstructed correctly with full

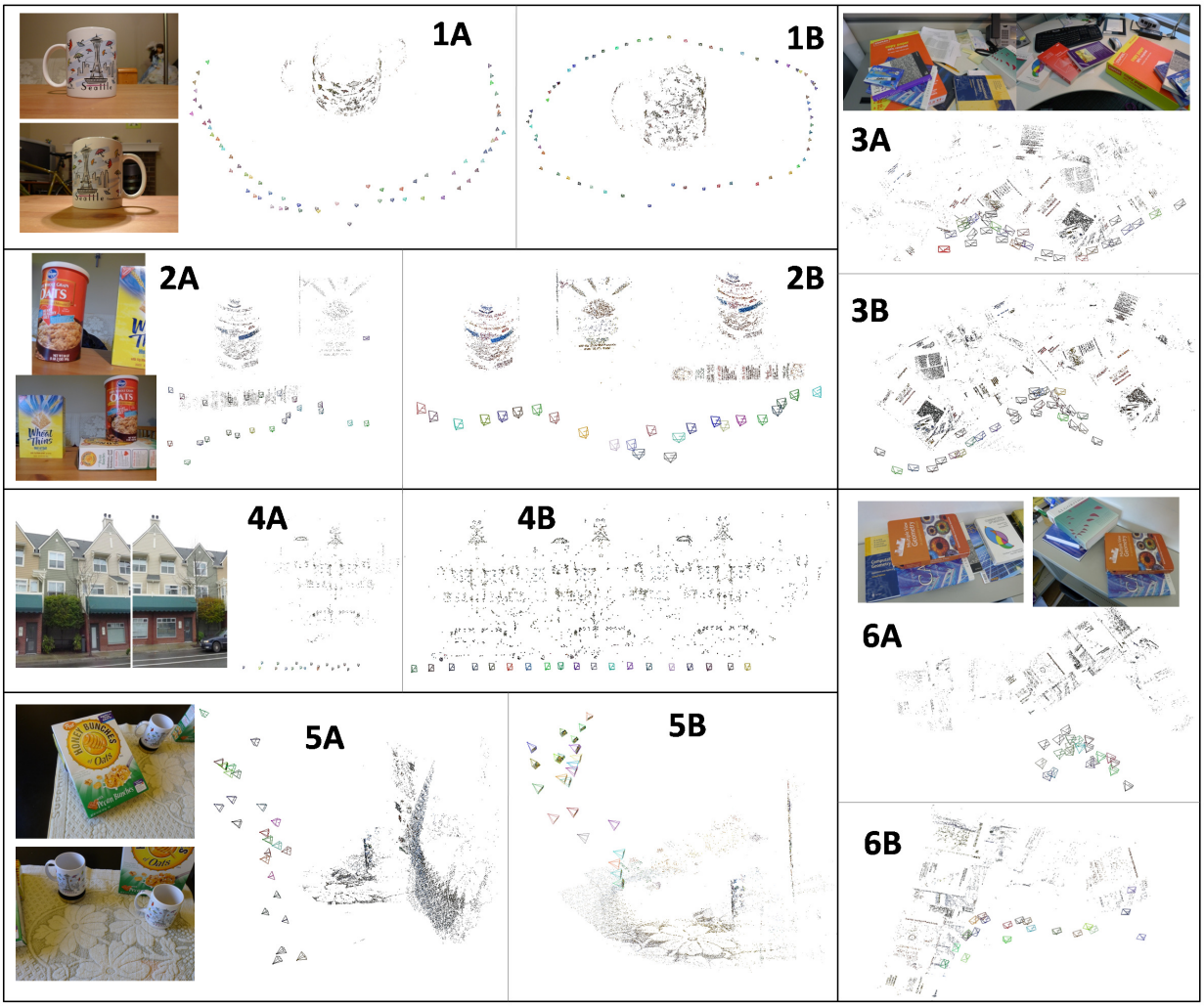

Figure 5: Reconstruction results on ambiguous datasets [20]. (A) using full view-graph, (B) using view-graph selected using our method. Datasets are in this order : (1) Cup, (2) Oats, (3) Desk, (4) Street, (5) Cereal, and (6) Books.

VGs as well, hence we omit them from comparison. The full VGs for these datasets are highly noisy (with ∼40%-50% outlier EGs) due to symmetry and presence of large duplicate objects. Due to high fraction of outlier EGs, we conservatively choose total flow value corresponding to 25% EG selection. It can be seen that with selected VGs, we are able to recover true structures for all and partially correct structure (better than full VG) for cereal dataset. Our reconstruction of cereal dataset is missing the second instance of the cup, possibly due to a complete lack of context features in many images of the isolated cup. Visualizations of selected VGs for these datasets and more details on failure case of 'cereal' are given in suppl. material. While these results are obtained using all priors, to show the effectiveness of disambiguation specific priors, we also reconstruct these datasets for VGs selected using *(i)* randomly assigned costs, and *(ii)* baseline priors based costs (tri. angle and homography). Table 3b shows whether the reconstruction is successful or not for all three cases of cost modeling.

Dataset	#Images
Alexander Nevsky Cath.	448
Arc de Triomphe	434
Radcliffe Camera	282
Church on Spilled Blood	277
Temple of Heaven	341
Pantheon Rome	782
Notre Dame Paris	715
St./ Peters Rome	1155

(a) #images in datasets

Dataset	R	B	A
cup	no	no	yes
oats	no	no	yes
desk	no	no	yes
books	no	no	yes
street	no	no	yes
cereal	no	no	no

(b) Reconstruction success

Table 3: (a) shows details of datasets, (b) shows reconstruction success for different cost modeling (R: randomly assigned costs, B : baseline priors based costs, A : all priors based costs).

Figure 6 shows the reconstruction results for three real

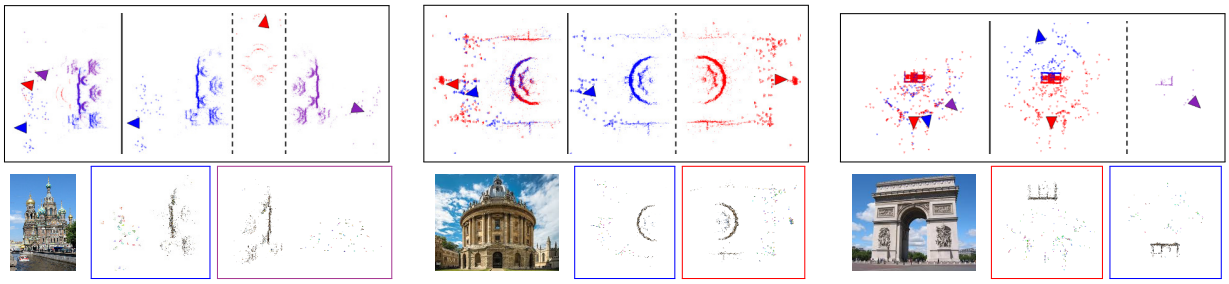

Church on Spilled Blood Radcliffe Camera Arc de Triomphe

Figure 6: Comparison of our reconstruction results with [13] for three datasets. The top left image for each experiment shows incorrect model reconstructed using the full VG, top right images show the correctly split models using the post-reconstruction pipeline of [13]. Bottom row shows a representative image for each dataset and our reconstruction results. Our splits are highlighted by color-coded boxes corresponding to [13]. Please see this figure in color.

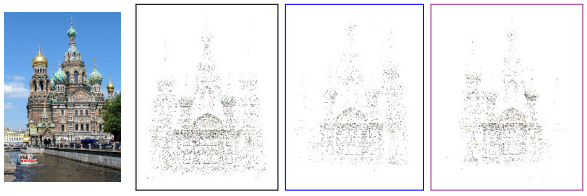

Figure 7: Front views of 'Church on Spilled Blood' reconstruction. This structure is asymmetric east to west (large gilded dome on the west side). Using full VG results in a symmetric facade with a ghost dome. Reconstruction with selected VG recovers two separate but correct models. From left to right : representative image, full VG model, selected VG split models.

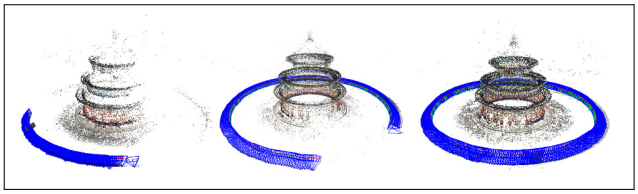

(a) Results from [22] : (left) reconstruction with *voc100* [10] VG (18466 EGs) and incremental SfM, (middle) reconstruction with *voc100* [10] VG (18466 EGs) and SfM method of [35], (right) reconstruction with consistent matching [22] based VG (2795 EGs) and incremental SfM.

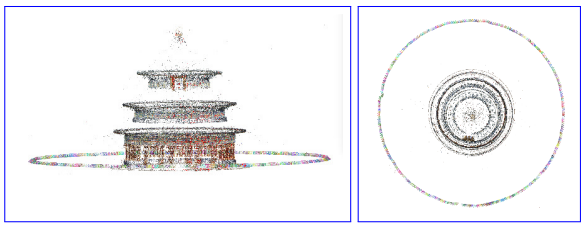

(b) Reconstruction with our selection (2697 EGs) and incremental SfM.

Figure 8: Reconstruction of 'Temple of Heaven' dataset.

world ambiguous scenes [13]. Method of [13] operates post-reconstruction to split incorrectly merged model parts and their processing takes ∼16 to ∼85 minutes for these datasets. Our framework pre-selects the view-graph and reconstruction is performed without any additional processing. Our subgraph selection framework is extremely efficient (takes 1–2 seconds for constructing and solving the MCNF problem for these datasets) and it is intended to be general purpose with disambiguation as one of the objectives. Figure 7 shows front views of full VG and selected VG reconstructions of 'Church on Spilled Blood' dataset. Our result on 'Alexander Nevsky Cath.' (shown in supp. material) is less cleanly split than [13].

Figure 8 shows the reconstruction of 'Temple of Heaven' dataset provided by [22]. It can be seen that despite starting from a full view-graph obtained with standard matching, the proposed VG selection method (with disambiguation priors based costs) is able to recover the correct structure. Please see supplementary material for additional results, visualizations, and discussions.

7. Conclusions and Future Work

In this paper we presented a novel unified framework for selecting subgraphs from initial view-graphs that provide better quality reconstructions even for highly ambiguous scenes. We show that objective specific priors can be incorporated to model image and pairwise selection costs in our framework and optimal selection can be obtained efficiently using an MCNF formulation. We utilize various priors based on local geometry such as overlap, local clustering coefficient, loop constraints etc. and show encouraging results on small and large datasets. Our main claim is that this framework provides a flexible platform and can potentially cater to a wider variety of variation in selection problem. In future, we would like to extend utility of our framework to other objectives such as sparsity or completeness by devising and incorporating relevant priors. It would also be interesting to learn the optimal values of hyper-parameters of this framework (weights for priors and normalization) by casting it as a learning problem.

References

[1] Sameer Agarwal, Noah Snavely, Ian Simon, Steven M. Seitz, and Richard Szeliski. Building rome in a day. In *Proceedings ICCV*, 2009. 1

[2] Avishek Chatterjee and Venu Madhav Govindu. Efficient and robust large-scale rotation averaging. In *2013 IEEE ICCV*, 2013. 1, 2

[3] D. Crandall, A. Owens, N. Snavely, and D. Huttenlocher. Discrete-continuous optimization for large-scale structure from motion. In *Proceedings IEEE CVPR*, 2011. 1, 2

[4] Jan-Michael Frahm, Pierre Fite-Georgel, David Gallup, Tim Johnson, Rahul Raguram, Changchang Wu, Yi-Hung Jen, Enrique Dunn, Brian Clipp, Svetlana Lazebnik, and Marc Pollefeys. Building rome on a cloudless day. In *Proceedings ECCV*, 2010. 1

[5] R. Gherardi, M. Farenzena, and A. Fusiello. Improving the efficiency of hierarchical structure-and-motion. In *Proceedings IEEE CVPR*, 2010. 1

[6] V. M. Govindu. Lie-algebraic averaging for globally consistent motion estimation. In *Computer Vision and Pattern Recognition, 2004. CVPR 2004. Proceedings of the 2004 IEEE Computer Society Conference on*, volume 1, pages I–684–I–691 Vol.1, June 2004. 2

[7] Venu Madhav Govindu. Robustness in motion averaging. In *Proceedings ACCV 2006*, pages 457–466, 2006. 2

[8] Richard Hartley and Andrew Zisserman. *Multiple View Geometry in Computer Vision*. Cambridge University Press, 2003. 4

[9] M. Havlena, A. Torii, J. Knopp, and T. Pajdla. Randomized structure from motion based on atomic 3d models from camera triplets. In *Proceedings IEEE CVPR*, 2009. 1

[10] Michal Havlena and Konrad Schindler. Vocmatch: Efficient multiview correspondence for structure from motion. In David Fleet, Tomas Pajdla, Bernt Schiele, and Tinne Tuytelaars, editors, *Proceedings ECCV 2014*. 2014. 8

[11] Michal Havlena, Akihiko Torii, and Tomas Pajdla. Efficient structure from motion by graph optimization. In *Proceedings ECCV 2010*. 2010. 2

[12] Jared Heinly, Enrique Dunn, and Jan-Michael Frahm. Recovering Correct Reconstructions from Indistinguishable Geometry. In *International Conference on 3D Vision (3DV)*, 2014. 1, 2

[13] Jared Heinly, Enrique Dunn, and Jan-Michael Frahm. Correcting for Duplicate Scene Structure in Sparse 3D Reconstruction. In *European Conference on Computer Vision (ECCV)*, 2014. 1, 2, 4, 6, 8

[14] Jared Heinly, Johannes Lutz Schönberger, Enrique Dunn, and Jan-Michael Frahm. Reconstructing the World* in Six Days *(As Captured by the Yahoo 100 Million Image Dataset). In *Computer Vision and Pattern Recognition (CVPR)*, 2015. 1

[15] N. Jiang, P. Tan, and L. F. Cheong. Seeing double without confusion: Structure-from-motion in highly ambiguous scenes. In *Computer Vision and Pattern Recognition (CVPR), 2012 IEEE Conference on*, pages 1458–1465, 2012. 1, 2, 4

[16] Yunpeng Li, Noah Snavely, and Daniel P. Huttenlocher. Location recognition using prioritized feature matching. In *Proceedings ECCV*, 2010. 6

[17] P. Moulon, P. Monasse, and R. Marlet. Global fusion of relative motions for robust, accurate and scalable structure from motion. In *IEEE ICCV*, 2013. 1, 2

[18] Carl Olsson and Olof Enqvist. Stable structure from motion for unordered image collections. In *in Proceedings of the 17th Scandinavian conference on Image analysis, ser. SCIA11*, pages 524–535, 2011. 1, 2

[19] Rahul Raguram, Changchang Wu, Jan-Michael Frahm, and Svetlana Lazebnik. Modeling and recognition of landmark image collections using iconic scene graphs. *International Journal of Computer Vision*, 95(3):213–239, 2011. 1, 2

[20] Richard Szeliski Drew Steedly Rick Szeliski Richard Roberts, Sudipta Sinha. Structure from motion for scenes with large duplicate structures. In *CVPR*, pages 3137–3144. Computer Vision and Patter Recognition, June 2011. 1, 2, 4, 6, 7

[21] Johannes Lutz Schönberger and Jan-Michael Frahm. Structure-from-motion revisited. In *IEEE Conference on Computer Vision and Pattern Recognition (CVPR)*, 2016. 1, 2

[22] Tianwei Shen, Siyu Zhu, Tian Fang, Runze Zhang, and Long Quan. *Graph-Based Consistent Matching for Structure-from-Motion*. 2016. 6, 8

[23] SudiptaN. Sinha, Drew Steedly, and Richard Szeliski. A multi-stage linear approach to structure from motion. In *Proceedings ECCV RMLE Workshop*. 2010. 1, 2

[24] Noah Snavely, Steven M. Seitz, and Richard Szeliski. Photo tourism: Exploring photo collections in 3d. *ACM Trans. Graph.*, 25(3), 2006. 1, 2, 6

[25] Noah Snavely, Steven M. Seitz, and Richard Szeliski. Modeling the world from internet photo collections. *Int. J. Comput. Vision*, 80(2), 2008. 2

[26] Noah Snavely, Steven M. Seitz, and Richard Szeliski. Skeletal graphs for efficient structure from motion. In *Proceedings IEEE CVPR*, 2008. 1, 2

[27] Christoph Strecha, Wolfgang von Hansen, Luc J. Van Gool, Pascal Fua, and Ulrich Thoennessen. On benchmarking camera calibration and multi-view stereo for high resolution imagery. In *IEEE Computer Society Conference on Computer Vision and Pattern Recognition (CVPR*, 2008. 6

[28] Chris Sweeney. *Theia Multiview Geometry Library: Tutorial & Reference*. University of California Santa Barbara., 2015. 6

[29] Chris Sweeney, Torsten Sattler, Matthew Turk, Tobias Hollerer, and Marc Pollefeys. Optimizing the viewing graph for structure-from-motion. In *Proceedings IEEE ICCV*, 2015. 2

[30] Roberto Toldo, Riccardo Gherardi, Michela Farenzena, and Andrea Fusiello. Hierarchical structure-and-motion recovery from uncalibrated images. *Computer Vision and Image Understanding*, 140:127 – 143, 2015. ISSN 1077-3142. 1, 2

[31] K. Wilson and N. Snavely. Network principles for sfm: Disambiguating repeated structures with local context. In *2013 IEEE International Conference on Computer Vision*, pages 513–520, Dec 2013. doi: 10.1109/ICCV.2013.69. 4

[32] Kyle Wilson and Noah Snavely. Robust global translations with 1dsfm. In *Proceedings ECCV*, 2014. 2

[33] Kyle Wilson, David Bindel, and Noah Snavely. When is rotations averaging hard? In *Proceedings of ECCV 2016*, October 2016. 2

[34] Changchang Wu. Towards linear-time incremental structure from motion. In *3DV Conference*, 2013. 1

[35] C. Zach, M. Klopschitz, and M. Pollefeys. Disambiguating visual relations using loop constraints. In *Computer Vision and Pattern Recognition (CVPR), 2010 IEEE Conference on*, pages 1426–1433, June 2010. 2, 8

[36] Christopher Zach, Arnold Irschara, and Horst Bischof. What can missing correspondences tell us about 3d structure and motion? In *2008 IEEE Computer Society Conference on Computer Vision and Pattern Recognition (CVPR 2008), 24-26 June 2008, Anchorage, Alaska, USA*, 2008. 1, 2, 4

A Unified View-graph Selection Framework for Structure from Motion

Rajvi Shah Visesh Chari P J Narayanan
Center for Visual Information Technology, IIIT Hyderabad, India
{rajvi.shah@research.iiit.ac.in, visesh@gmail.com, pjn@iiit.ac.in}

Supplementary Material

1. Summary

This supplementary document provides additional information about the following, (i) Implementation details (ii) Explanation of the synthetic view-graph based experiments. (iii) Qualitative results (point clouds) amd analysis of selection statistics for Internet Landmarks dataset [5, 3]. (iv) Visualizations of the selected view-graphs for small ambiguous scenes dataset [4]. (v) Reconstructions of small ambiguous scenes dataset [4] with individual pairwise priors based selection. (vi) Larger versions of results for large ambiguous datasets given in the main paper.

2. Implementation details

We use David Lowe's implementation[1] for SIFT feature detection and descriptor computation, and approximate near neighbour (Kd-tree based) approach[2] with ratio-test for feature matching. These components are standard in SfM community. We use Theia SfM library[3] for relative pose estimation, geometric verification of matches, and for computing geometry based (pairwise and tripletwise) priors. For MCNF based optimization, we use Mosek optimization library[4] with C++ interface. The optimization is done efficiently using the Network Simplex method.

All disambiguation results use incremental SfM (VisualSfM) based reconstructions. Results on Landmarks datasets use global SfM based reconstructions as we want to compare accuracy of these reconstructions with respect to incremental SfM based baseline reconstructions. We use Theia's implementations of robust rotation averaging [1] and 1D translation estimation [6] as global SfM pipeline.

All CPU based experiments (MCNF optimization and global SFM reconstructions) are run single-threaded on a machine with Intel Xeon 2.50GHz processor and 12GB RAM. For VisualSfM based reconstructions, we use a similar machine with NVidia 970 GPU.

We will make our codes for prior computation, cost modeling, and network based optimization, publicly available along with the paper.

[1] http://www.cs.ubc.ca/~lowe/keypoints/siftDemoV4.zip
[2] https://www.cs.umd.edu/~mount/ANN/Files/1.1.2/ann_1.1.2.zip
[3] http://www.theia-sfm.org/
[4] https://www.mosek.com/

3. Experiments with synthetic view-graphs

To systematically study the effect of flow parameter on sub-graph selection, we solve the proposed MCNF problem for a large number of synthetic graphs. The results of this experiment are shown and discussed in the main paper (Section 5, Figure 4) . We construct the synthetic graphs to simulate connectivity of real-world unorganized image collections using the below process,

1. Begin with the number of vertices (N) in the graph and average degree (d_{avg}) as a fraction of N.
2. The degree of each vertex is sampled from a Gaussian distribution with $\mu = d_{avg}$ and varying σ.
3. The adjacency list of each vertex is also created by sampling a Gaussian distribution. For a vertex i, the d_i connected vertices are sampled from a Gaussian distribution with $\mu = i$ and σ as a function of average degree (d_{avg}). When vertex i is sampled, we randomly choose between vertices $i-1$ and $i+1$ for ensuring validity of edges.
4. The vertices are assumed to be arranged, in a linear fashion (e.g, capturing a facade or a street), and in a loop (e.g, capturing around a building or a block). For loopy configuration, we use modulo for defining vertex adjacency.
5. After defining the connections, each edge is randomly assigned a cost between -1 and 0.
6. Finally, the vertices are shuffled randomly to simulate the unorganized nature of SfM view-graphs.

We vary the number of vertices from 100 to 5000 in multiples of 2, the average degree from 5% to 40% in multiples of 5, and loopy/linear arrangement to obtain synthetic graphs with a wide range of scale and connectivity. In most Internet collection view-graphs, many images come from popular viewpoints; these images have higher degree in the graph and are more likely connected to other adjacent images. While images corresponding to less popular viewpoints also exist in the datasets with fewer connections to popular viewpoint images. This scenario is well captured by our Gaussian sampling and neighbourhood assumptions in our simulation. Hence, the synthetic view-graphs are good approximations of connectivity in real-world unorganized community photo collections. In Figure 2, we show the effect of varying total flow on selection statistics. It can be seen that observations on Internet landmark datasets are similar to that of the synthetic graph experiments (Figure 4 in the main paper).

4. Internet landmarks reconstructions

We used our VG selection framework on three large unorganized Internet datasets of popular landmark sites (statistics given in the main paper Section 6, Table 2). We reconstruct the scenes using selected view-graphs and full view-graphs with global SfM pipeline (typically slightly less robust than incremental SfM methods) in order to compare the reconstruction accuracy w.r.t. incremental SfM based baseline reconstructions. To understand the effect of total flow parameter on selection and reconstruction, we plot the selection and reconstruction statistics for increasing value of total flow parameter in Figure 2.

The quantities $|V_s|/|V|$, $|N_c|/|V|$, and $|E_s|/|E|$ indicate the fraction of total vertices selected, fraction of total vertices reconstructed, and fraction of total edges (EGs) selected. The rotation and translation errors (R_{err} and T_{err}) are divided by max. to bring these in the same range. As it can be seen, fraction of reconstructed vertices remain close to the fraction of selected vertices at all levels of selections. This result indicates that the selection scheme naturally endorses connectity. This is a result of using only encouraging costs for selection that prefers to select longer chains over disjoint segments. Also most vertices are reconstructed and the reconstruction errors are stable at much lower value of flow (and selected pairs) than full VG. The flow value is on a logarithmic scale for a better depiction. It can be also seen that for all three datasets the pair selection vs. flow curve behaves very similarly to the synthetic view-graphs. This result validates our choice of using synthetic view-graph based selection statistics to determine the flow parameter value in practice. The selected VG reconstructions and full VG reconstructions are qualitatively similar or better (shown in Figure 1). Notice the ghosting in Notre Dame dataset disappear in selected VG based reconstruction.

5. VG selection for small ambiguous scenes

In the paper, we showed utility of our method for selecting view-graphs that lead to accurate and ghost-free reconstructions of highly ambiguous scenes [4]. For all selections, we model costs using all priors (including disambiguation priors) with equal weights. Since these datasets are small (20 to 70 images) and expectedly have a very high fraction of outlier EGs (40% to 60%), we use conservative values of total flow for sparse subgraph selection. Here, we visualize the selected subgraphs by overlaying the edges corresponding to the selected EGs on reconstructed point clouds and cameras. We omit 'Street' dataset here, as it is difficult to visually compare view-graphs due to 1D arrangement of its cameras.

The full VGs (after putative matching and geometric verification) consist of nearly 50% wrong EGs for these datasets, resulting in ghosting errors. The selected VGs have a few incorrect EGs, however, SfM methods are robust to overcome a small fraction of inaccurate EGs, and produce correct reconstructions.

6. Effect of individual priors on small ambiguous scenes reconstruction

In the paper, we explained six pairwise priors (existing and new) that can be useful to achieve different selection objectives (accuracy and disambiguation). Our main results are obtained by using a (uniform) weighted combination of all six priors. Here, we show that each prior has a different effect on selection and in turn the reconstruction. Also that individual priors are often not strong enough to lead to ghost-free reconstruction of ambiguous scenes whereas combining priors lead to accurate and ghost-free reconstructions. Figure 4 and Figure 5 show the reconstructions with selections based on each individual pairwise prior.

Consider the *Oats* dataset results. It can be seen that the VGs selected corresponding to Infinite Homography, Overlap, Context Measure, and Loop Consistency enable to disambiguate the two instances of the 'Oat box' more as compared to the Triangulation Angle and Multiple Motions priors, resulting in relatively more complete and correct reconstructions of the scene. For *Cup* dataset, no prior standalone can recover the correct motion (camera arrangement). However, it can be seen that reconstructions with different priors recover different areas correctly or incorrectly. For *Cereal* dataset, where combining all priors result in a partially incorrect reconstruction (shown in main paper), using only Overlap based prior or Loop Consistency prior lead to correct reconstructions. Ideally, optimal combination of priors would ensure best reconstruction results. This is a non-trivial hyper-parameter optimization/learning problem that remains the focus of our future work.

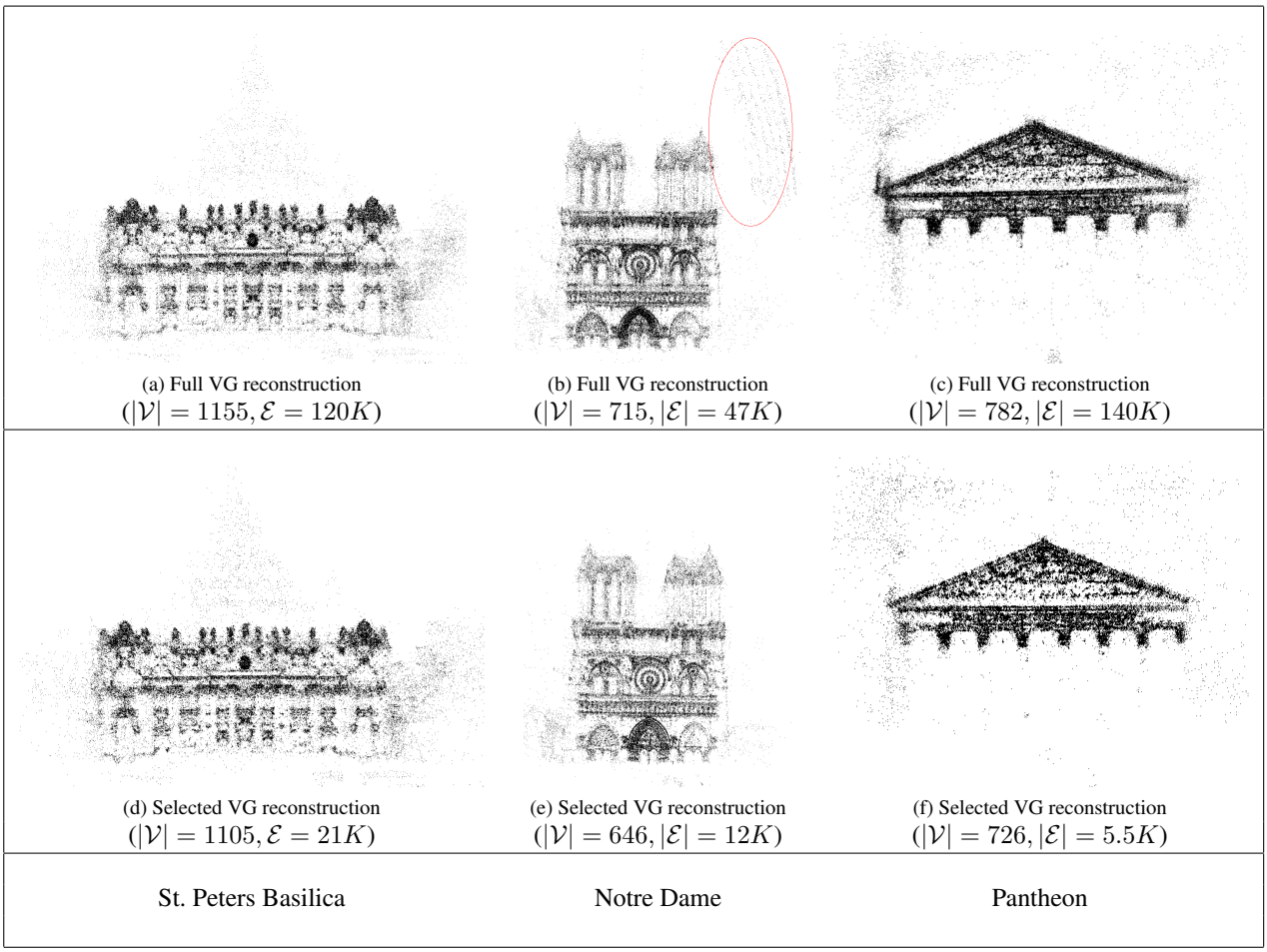

(a) Full VG reconstruction ($|\mathcal{V}| = 1155, \mathcal{E} = 120K$)

(b) Full VG reconstruction ($|\mathcal{V}| = 715, |\mathcal{E}| = 47K$)

(c) Full VG reconstruction ($|\mathcal{V}| = 782, |\mathcal{E}| = 140K$)

(d) Selected VG reconstruction ($|\mathcal{V}| = 1105, \mathcal{E} = 21K$)

(e) Selected VG reconstruction ($|\mathcal{V}| = 646, |\mathcal{E}| = 12K$)

(f) Selected VG reconstruction ($|\mathcal{V}| = 726, |\mathcal{E}| = 5.5K$)

St. Peters Basilica | Notre Dame | Pantheon

Figure 1: Renders of point clouds for full VG and selected VG reconstructions of Internet landmarks datasets. Notice the ghosting in Notre Dame reconstruction with full view-graph (highlighted by a red oval), the reconstruction with selected view-graph is free from ghosting.

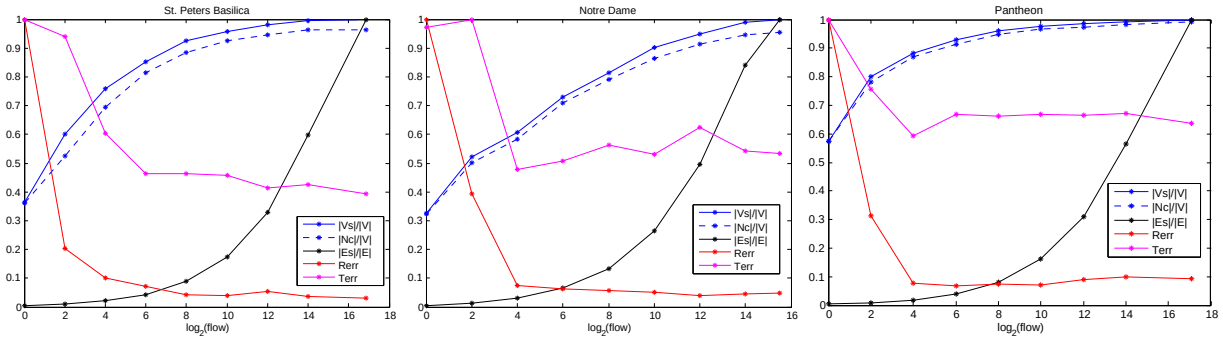

(a) St. Peters Basilica (b) Notre Dame (c) Pantheon

Figure 2: View-graph selection and reconstruction statistics with increasing values of flow for three datasets. The quantities $|V_s|/|V|$, $|N_c|/|V|$, and $|E_s|/|E|$ indicate the fraction of total vertices selected, fraction of total vertices reconstructed, and fraction of total edges (EGs) selected. The rotation and translation errors (R_{err} and T_{err}) are divided by max. values to bring these in the same range. These plots are explained in section 4.

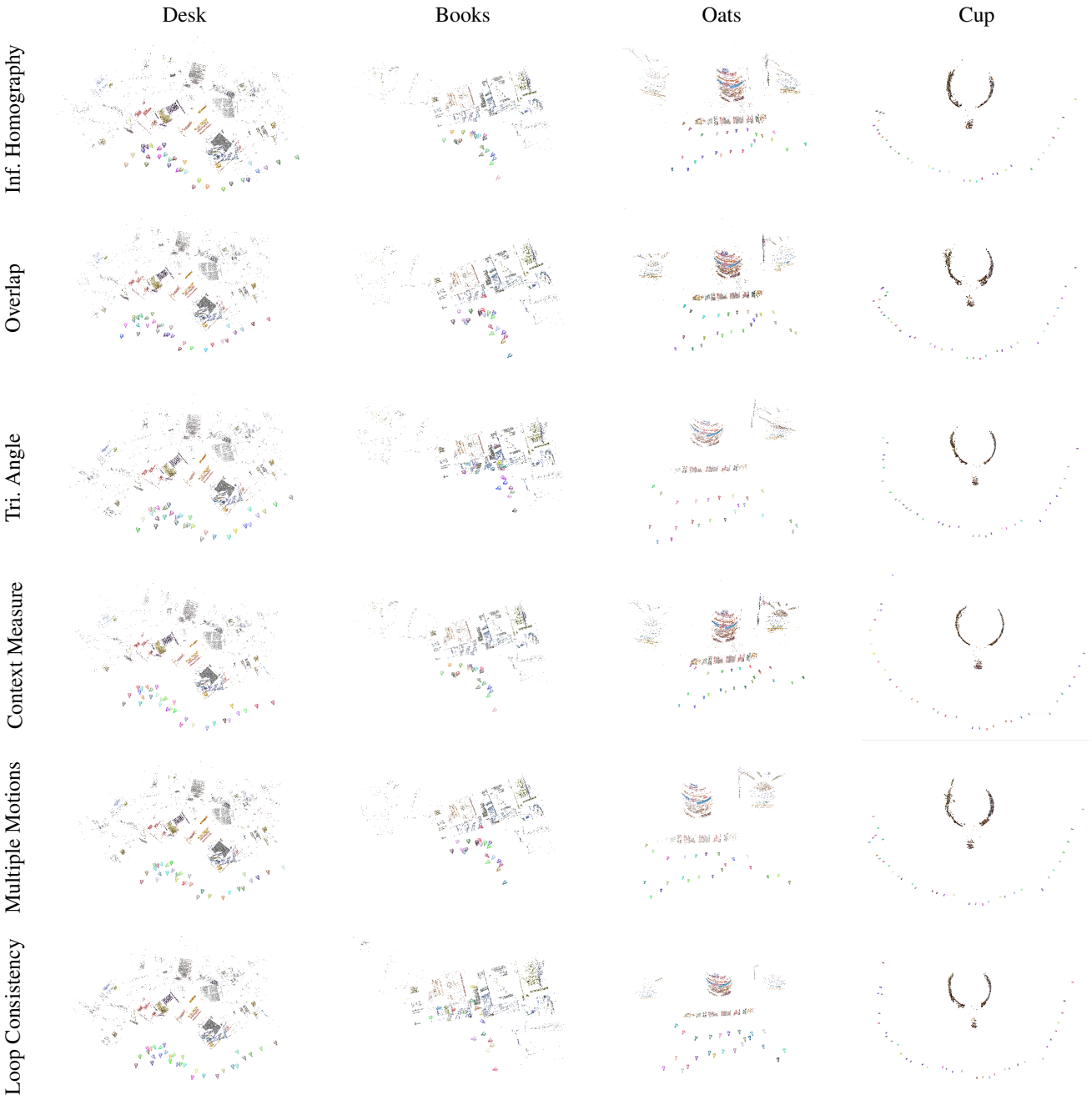

Figure 5: Reconstruction results with selection based on individual priors for 'Desk', 'Books', 'Oats', and 'Cup' datasets

References

[1] A. Chatterjee and V. M. Govindu. Efficient and robust large-scale rotation averaging. In *2013 IEEE ICCV*, 2013. 1

[2] J. Heinly, E. Dunn, and J.-M. Frahm. Correcting for Duplicate Scene Structure in Sparse 3D Reconstruction. In *European Conference on Computer Vision (ECCV)*, 2014. 6

[3] Y. Li, N. Snavely, and D. P. Huttenlocher. Location recognition using prioritized feature matching. In *Proceedings ECCV*, 2010. 1

[4] R. Roberts, S. Sinha, R. Szeliski, D. Steedly, and R. Szeliski. Structure from motion for scenes with large duplicate structures. In *CVPR*, pages 3137–3144. Computer Vision and Patter Recognition, June 2011. 1, 2, 5

[5] N. Snavely, S. M. Seitz, and R. Szeliski. Photo tourism: Exploring photo collections in 3d. *ACM Trans. Graph.*, 25(3), 2006. 1

[6] K. Wilson and N. Snavely. Robust global translations with 1dsfm. In *Proceedings ECCV*, 2014. 1

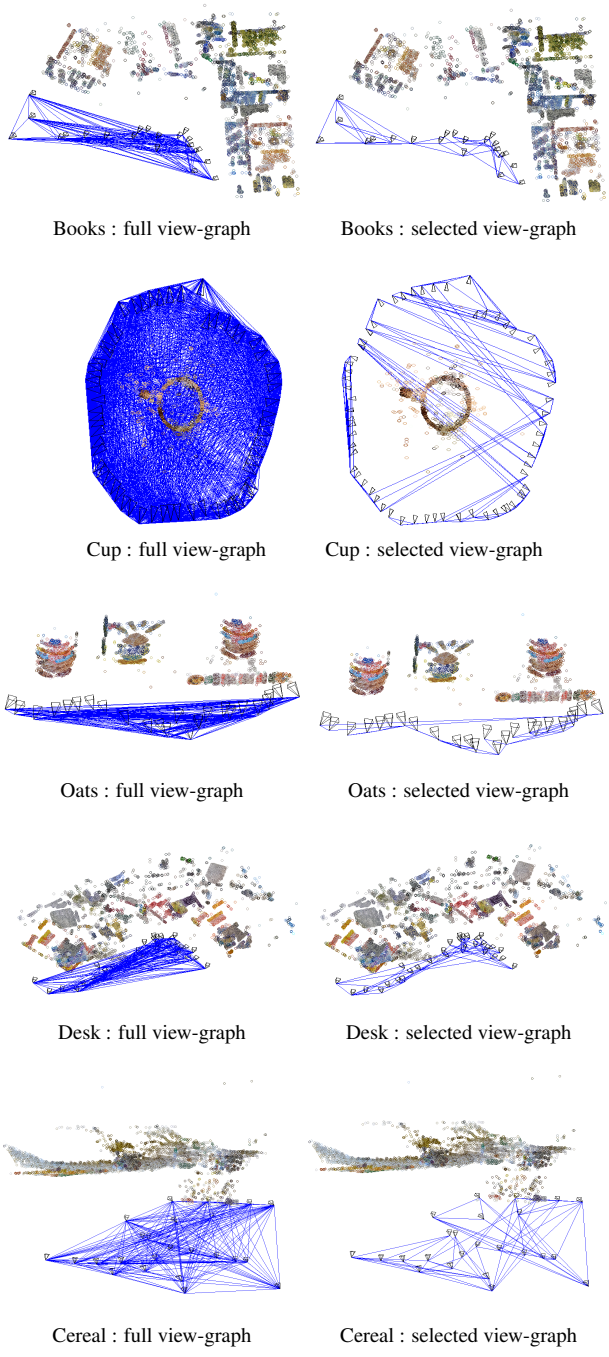

Figure 3: Full view-graphs (left) and selected view-graphs (right) for small ambiguous scenes dataset [4]. Please observe the outlier EGs in selected VGs are far fewer as compared to the high amount of outlier EGs in full VGs.

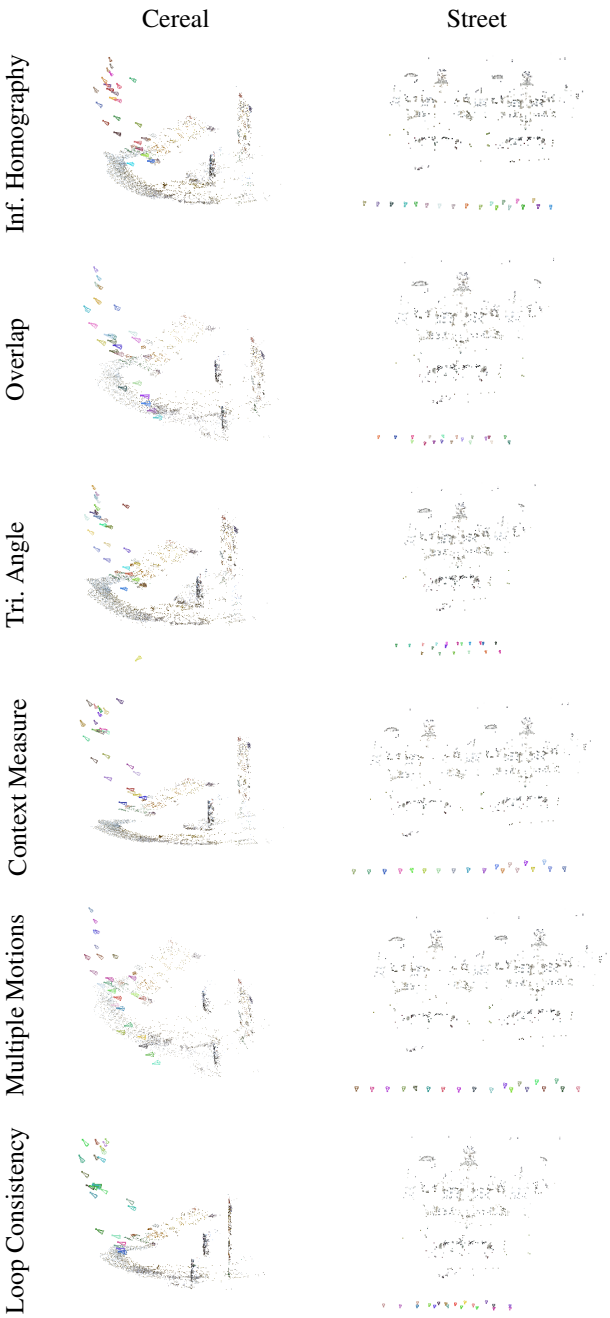

Figure 4: Reconstruction results with selection based on individual priors for 'Cereal' and 'Street' datasets

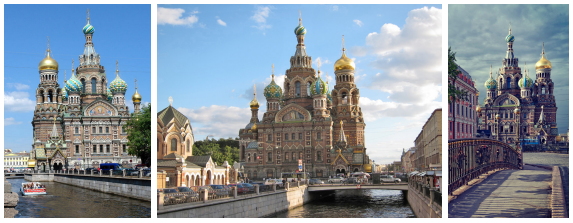

Representative images of the monument

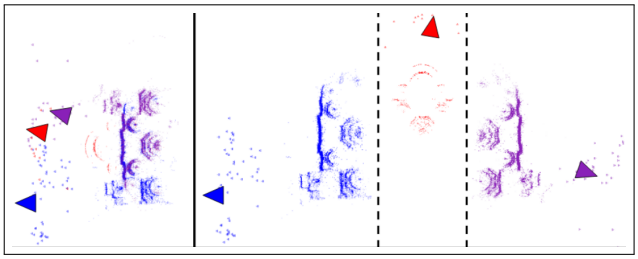

Result of [2] : (left) wrong reconstruction with full view-graph, (right) three correctly split models shown in distinct colors. Takes 1.4 hours to post-process the wrong reconstruction.

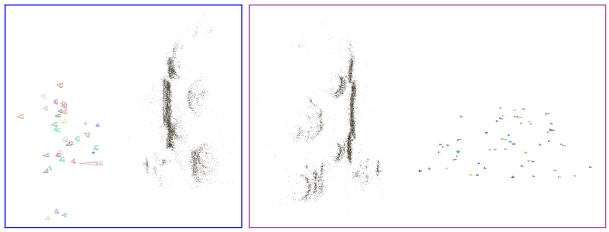

Reconstruction with selected view-graph (ours) results into two correct smaller models (highlighted in corresponding colors). Our view-graph selection takes 2-4 seconds.

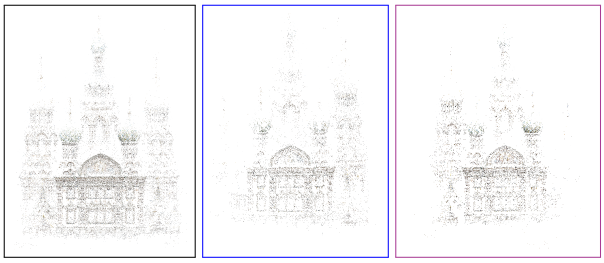

Front views : reconstruction result of full VG (left), reconstruction result of selected VG, split into two models (right)

Figure 6: Reconstruction of 'Church on Spilled Blood' dataset. This structure is asymmetric east to west (large gilded dome on the west side). Using full VG results in a symmetric facade with a ghost dome. Reconstruction with selected VG recovers two separate but correct models.

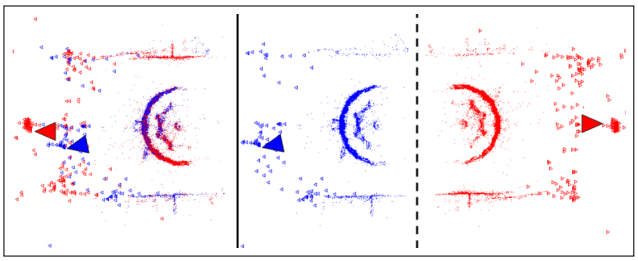

Result of [2] : (left) wrong reconstruction with full VG, (right) correctly split two models. Time ∼31 min. to post-process.

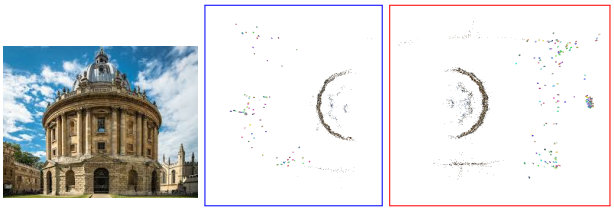

Representative image (left). Reconstruction with selected VG (ours) results into two correct models. Time ∼2 sec.

Figure 7: Reconstruction of 'Radcliffe Camera', a structure with rotational symmetry. Using full VG, it incorrectly gets folded vertically. Reconstruction with selected VG recovers two separate but correct models.

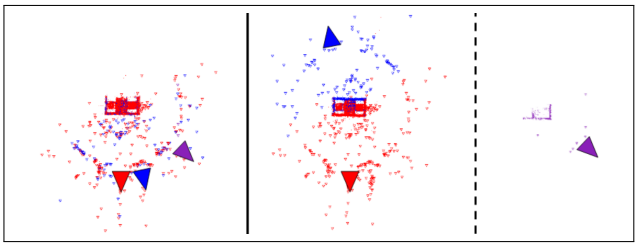

Result of [2] : (left) wrong reconstruction with full VG, (right) correctly split and merged models. Time ∼16 min. to post-process.

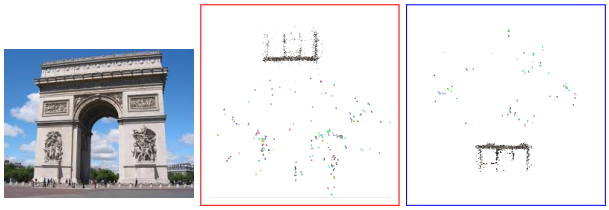

Representative image (left). Reconstruction with selected VG (ours) results in two correct models. Time ∼2 sec.

Figure 8: Reconstruction of 'Arc de Triomphe' dataset.